energies

MDPI

Article

Hierarchical Distributed Motion Control for Multiple Linear Switched Reluctance Machines

Bo Zhang [1,2], Jianping Yuan [2], Jianjun Luo [2], Xiaoyu Wu [1], Li Qiu [1] and J.F. Pan [1,*]

[1] College of Mechatronics and Control Engineering, Shenzhen University, Shenzhen 518060, China; zhangbo@szu.edu.cn (B.Z.); wuxy@szu.edu.cn (X.W.); qiuli@szu.edu.cn (L.Q.)

[2] Laboratory of Advanced Unmanned Systems Technology, Research Institute of Northwestern Polytechnical University in Shenzhen, Shenzhen 518060, China; jianpingyuan@yeah.net (J.Y.); jjluo@nwpu.edu.cn (J.L.)

* Correspondence: pjf@szu.edu.cn; Tel.: +86-755-2653-5382

Received: 14 June 2017; Accepted: 25 August 2017; Published: 16 September 2017

Abstract: This paper investigates a distributed, coordinated motion control network based on multiple direct-drive, linear switched reluctance machines (LSRMs). A hierarchical, two-level synchronization control strategy is proposed for the four LSRMs based motion control network. The high-level, reference signals agreement algorithm is first employed to correct the asynchronous behaviors of the position commands. Then, the low-level tracking synchronization method is applied for the collaborative position control of the four LSRMs. The proposed two-level, fault-tolerant control strategy eliminates the asynchrony of the reference signals and it also guarantees the coordinated tracking control performance of the four LSRMs. Experimental results demonstrate that effective coordinated tracking control can be ensured, based on the successful agreement of reference signals and an absolute tracking error falling within 2 mm can be achieved.

Keywords: linear switched reluctance machine; coordinated motion control network; signal agreement; tracking synchronization

1. Introduction

In industrial manufacture environment, there are many collaborative operations for multiple working units to realize one ultimate task. The distributed working units, which are often driven by electric machines, are often required to operate cooperatively. For example, in a processing line with multiple linear operations, as shown in Figure 1, the entire processing task for the workpiece requires one drilling machine, one screwing machine, one welding machine, and one painting machine to finish the job. Traditionally, the processing task is realized in a sequenced manner, i.e., each machine cannot execute until its former machine is settled. If there occurs any positioning error from any of the linear processing machines, then the entire precision is bound to deteriorate and the entire control performance will be affected. The overall processing task even collapses if any process fails [1]. If each linear machine can form as an individual motion control system and it has the controller, sensor, and drives of its own, then the linear machines can work cooperatively by the communications among the local controllers from each linear machine, then the ultimate global task for the processing job can be accomplished, without requiring any high-level supervisory administration or decision [2].

Since each linear machine belongs to the individual positioning control system locally, the machine accesses its individual reference signal. Therefore, each linear machine should be guided by its reference signal for correct positioning operations. This is because an appropriate motion control of electric machines depends on the external, reference signals of their own as a prerequisite. Positioning operations inevitably suspend from the electric machines if the reference signals are interrupted [3].

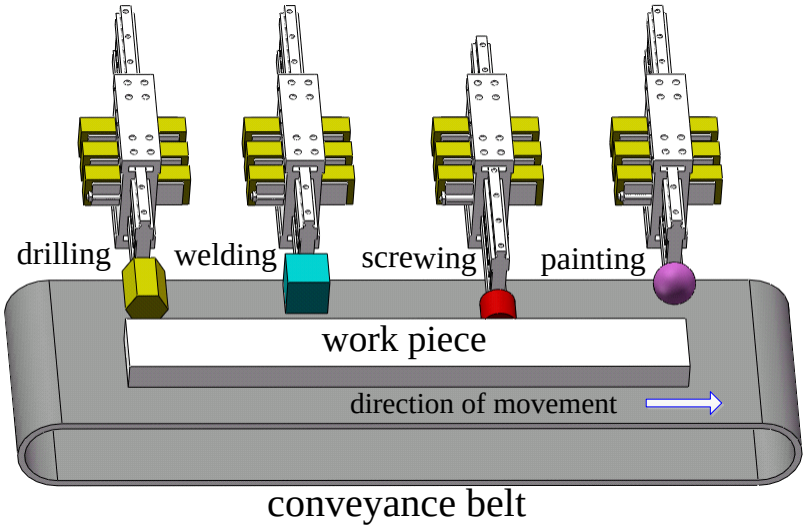

Figure 1. Concept of the processing line.

For the multi-processing line, the motion profiles of all the linear machines should first be synchronized to realize one ultimate tracking synchronization goal. Otherwise, if there occurs a breakdown or delay of one machine for a period of time, other linear machines will definitely fall into disorder. Since the four linear machines are led by four reference signals, there unavoidably occurs motion coordination failure if the four reference signals of the different machines are independent and unrelated from each other. In other words, if unexpected deviations among the independent reference signals exist, the motion of all the linear machines cannot be synchronized unless their reference signals are agreed first.

Up till now, there is rare literature regarding the tracking synchronization of multiple linear direct-drive machines, especially on the reference agreement of electric machines. Current coordination strategies focus on the design and optimization of the lower-level, cooperative tracking control algorithms to improve the relative error behaviors among all working units [2,3]. However, since tracking coordination control cannot affect the external, independent reference signals, the relative error behaviors may deteriorate and the tracking control algorithms even malfunction if all the working units are driven by unrelated, asynchronous reference signals [4]. The correction of the asynchronous behaviors from multiple reference signals and the coordinated tracking of multiple units can be similarly considered as the agreement or consensus problem [5]. Article [6] reviews some recent progress and results in the coordination and synchronization control of multi-agent networks, which can be categorized into the main research directions as formation, optimization, and estimation, etc. The effectiveness of the interaction within a consensus networked control system is discussed from the standpoint of its controllability properties [7]. In [8], consensus control is employed in the pattern formation for various kinds of vehicles. The distributed coordination protocol design for multi-agent systems with general linear dynamics and directed communication graphs is addressed in [9], based only on the agent dynamics and the relative states of neighboring agents. Qu etc. proposes a framework based on matrix theory to analyze and design cooperative control algorithms for a group of vehicles, interacting with each other locally [10]. A second-order coordinated tracking problem of multiple three-degrees-of-freedom laboratory helicopters is studied on directed communication topologies to combat model nonlinearity and uncertainty [11]. Nevertheless, the above mentioned research work demonstrates the effectiveness of the coordinated control methods theoretically and the performance of the networked control systems is barely analyzed quantitatively.

For high-precision, one dimensional translational applications, the scheme of direct-drive linear machines are advantageous over the solution of rotary motors coupled with mechanical

transmissions, since linear machines have fast response, high reliability, and the annihilation of backlashes, accumulated errors, etc. [12]. A linear switched reluctance machine (LSRM), which consists of only silicon-steel plates and windings with no permanent magnet (PM) involved, is particularly suitable for the operation under hostile environment. Compared to linear PM synchronous machines, the LSRM is more cost-effective, owing to its robust and stable mechanical structure. Therefore, the overall system cost for the implementation of a coordinated linear motion control network is low [13].

Current research mainly concentrates on optimized machine design and control performance improvement of single switched reluctance machine based motion control systems [14–17]. In [14], a double-sided, asymmetric LSRM structure is proposed to ensure a higher force-to-volume ratio with more acceleration, compared to a double-sided, symmetric counterpart with the same dimensions and ratings [18]. For the performance enhancement from the control aspect, a nonlinear proportional differential controller is introduced for the real-time LSRM based suspension system to achieve a better dynamic response [17]. An adaptive controller is proposed to combat the difficulties and uncertain control behaviors for a double-sided LSRM in [18], etc.

For the multi-procedure processing line, the asymmetric LSRMs with more force-to-volume ratio are more efficient than their symmetric counterparts. When multiple LSRMs are prompted cooperatively to achieve one desired synchronization goal, the entire network should first be led by a coordinated reference signal. Otherwise, each LSRM is compelled to follow its own reference signal and a synchronized motion of the four LSRM cannot be achieved. Meanwhile, the coordinated tracking control of the four LSRMs should also be included to improve the control performance of the entire network at the same time.

To tackle the problems discussed above, this paper first constructs a hierarchical, two-level synchronized motion control framework for the four distributed LSRMs based motion control network. The framework consists of two control levels: the reference signals agreement module and the coordinated tracking control module. The upper-level reference signal coordination module is employed to agree the reference signals for each LSRM and the function of the lower-level coordinated tracking control module is to supervise each LSRM to track the reference signal coordinately.

The innovation of the paper can be summarized as follows. First, distributed motion synchronization is investigated based on four independent, direct-drive, asymmetric LSRMs for the potential applications of the multi-procedure processing line with the ability of cooperative operations. Second, a two-level, hierarchical, synchronization motion control scheme is realized for the proposed LSRMs network. Third, performance analysis proves that the proposed hierarchical control strategy is superior to both the lower-level coordination synchronization alone of the four LSRMs network.

2. Theoretical Background

2.1. LSRM Modeling

The machine structure can be found in Figure 2a,b. It employs an asymmetric structure to achieve a higher force-to-volume ratio [14] and the double-sided machine structure further ensures a more stable and reliable output performance [18]. The LSRM consists of six stators with windings that forms phases AA′, BB′, and CC′. Instead of perfect mirroring along the moving platform, phase A from the upper axis corresponds to phase A′ at the lower right corner of the axis, phase B to B′ and phase C to C′, respectively. The teeth from the moving platform are not symmetric either. They appear alternatively along each side of the axis of the moving platform.

Major machine specifications can be found in Table 1. The four LSRMs can be regarded as identical control objects with the same dimensions and ratings.

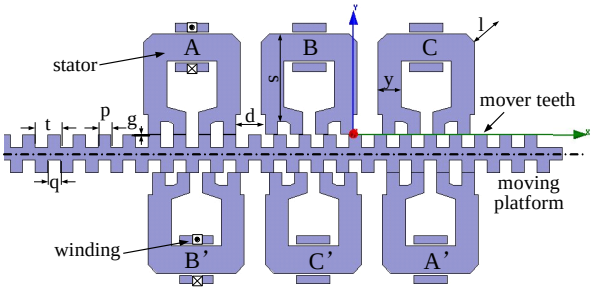

(a)

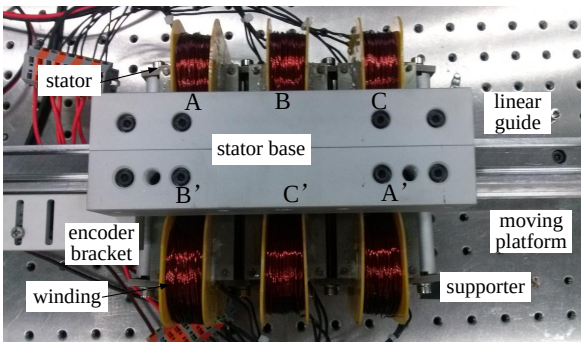

(b)

Figure 2. (**a**) machine structure and (**b**) picture.

Table 1. Main Specifiations of LSRM.

Quantity	Value
Mass of moving platform	3.8 kg
Mass of stator	5.0 kg
Pole pitch	12 mm
Pole width	6 mm
Air gap length	0.3 mm
Phase resistance	2 Ohm
Number of turns	200
Stack length	50 mm
Rated power	250 W
Voltage	50 Volt
Encoder resolution	1 µm

The kinetic equation that governs the behavior of the i-th LSRM based motion control system can be represented as [12] :

$$m_i \frac{d^2 x_i}{dt^2} + B_i \frac{dx_i}{dt} + fl_i = f_i \tag{1}$$

where m_i, x_i, B_i, fl_i, and f_i are the mass, position, friction coefficient, load force, and the electromagnetic force for the i-th LSRM, respectively. The i-th LSRM can be described in the voltage equation as,

$$u_{i_k} = R_{i_k} i_{i_k} + \frac{d\Lambda_{i_k}}{dt}, \quad (k = A, B, C) \tag{2}$$

where u_{i_k} ,R_{i_k}, and i_{i_k} are the terminal voltage, coil resistance, and current, respectively. Λ_{i_k} represents the flux-linkage for the k-th winding.

2.2. Network Topology and Graph Theory

The LSRMs network can be mathematically abstracted as a *graph*, which is composed of a set of nodes and edges. In particular, given a coordinated network of N interconnected LSRMs, let the *graph* be denoted by $G = \{V, E\}$, where the *node* set $V = \{1, \ldots, N\}$ is a collection of all LSRMs and the *edge* set $E \subset V \times V$ describes the topology of the interconnected network among the LSRMs. An edge exists between node i and j (denoted by $(i, j) \in E$), if there is an information flow among these nodes. The *directed edge* from node i to j denotes that node j can obtain the information from node i only and the *directed graph* can be formed by the set of such directed edges. A *directed path* is a sequence of directed edges in a directed graph and a *directed tree* is a directed graph in which there is only one node, called the root, which has solely one directed path to all other nodes. A *cycle* is a directed path that forms a closed loop [19].

A *subgraph* of $G = \{V, E\}$ is a graph such that the sets of the nodes and edges are the subsets of $\{V, E\}$. A *directed spanning tree* G_t of $G = \{V, E\}$ is a subgraph of G such that G_t is a directed tree and it has the same nodes as G. The *adjacency matrix* $A = [a_{ij}]$ associated with G is defined as $a_{ij} = 1$ if $(i, j) \in E$ and $a_{ij} = 0$ if $(i, j) \notin E$. The *Laplacian matrix* associated with graph G is denoted as $L = [l_{ij}]$, where $l_{ii} = \sum a_{ij}$ and $l_{ij} = -a_{ij}$, $i \neq j$, $i, j = 1, \cdots, N$.

For example, the directed graph of four LSRMs based motion control systems can be illustrated in Figure 3 and the network topology shows that node 0 is the root and node 1–3 receive the directed information from node 0. Nodes 1 and 2 can communicate with each other while node 3 receives the information from node 0 only. Figure 3b is a subgraph and it forms a directed spanning tree from the graph depicted in Figure 3a,c is a cycle.

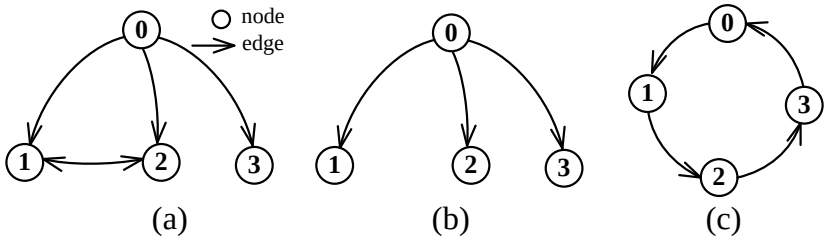

Figure 3. Node and edge of graph: (**a**) directed graph, (**b**) tree, and (**c**) cycle.

3. Control Strategy

3.1. Reference Signal Consensus Module

To realize reference signals agreement, a first-order consensus algorithm is adopted. Sinusoidal waveforms are selected as the reference signals and the initial phase φ (rad), angular frequency ω (rad/s), and amplitude A (mm) are represented as the agreement variables of the reference signals. The first-order consensus algorithm serves as the distributed feedback [20] and is responsible for the correction of variable φ, ω, and A to realize reference signal agreement.

The regulation processing of the three variables is modeled as single-integrator dynamics and the reference signals agreement algorithm for the i-th reference signal can be expressed as [21],

$$\dot{p}_i = -\sum_{j=1}^{N} \hat{a}_{ij} \left(p_i - p_j \right), i = 1, \ldots, N \tag{3}$$

where $p_i = \begin{bmatrix} \omega_i & A_i & \varphi_i \end{bmatrix}^T$ denotes the variable vector of the i-th reference signal and $\hat{a}_{ij}$ is the (i, j) entry of the adjacency matrix $\hat{A} \in R^{N \times N}$ associated with the network topology of the interactions with all reference signals based on the consensus algorithm. The necessary and sufficient condition

that guarantees the convergence of the closed loop dynamics governed by the consensus algorithm can be found in [21]. It can be proved that all variables states of the reference signals converge to one common value by algorithm (3) if and only if the graph modeling the communication topology contains a directed spanning tree.

3.2. Unit System Control

For each LSRM based unit system, the dual-loop control strategy is applied. The outer loop is a position control and the inner is a current loop, respectively. The current control loop is responsible for correct current tracking and it derives the actual current output for each phase with proper response time and precision. Meanwhile, the current control loop is much faster than the position loop with a perfect tracking capability [17]. The multi-phase excitation with a look-up table linearization scheme is employed to combat the nonlinearities of the LSRMs. The control diagram can be depicted as shown in Figure 4. For the i-th LSRM based unit system, position error e_i is decided from the difference between the command x_i^* and the actual position x_i of i-th LSRM, along with the difference information from the j-th machine e_j. The position controller then calculates the control input f_j and the multi-phase excitation with the look-up table linearization scheme determines the current command for the k-th winding, according to the current position of the machine.

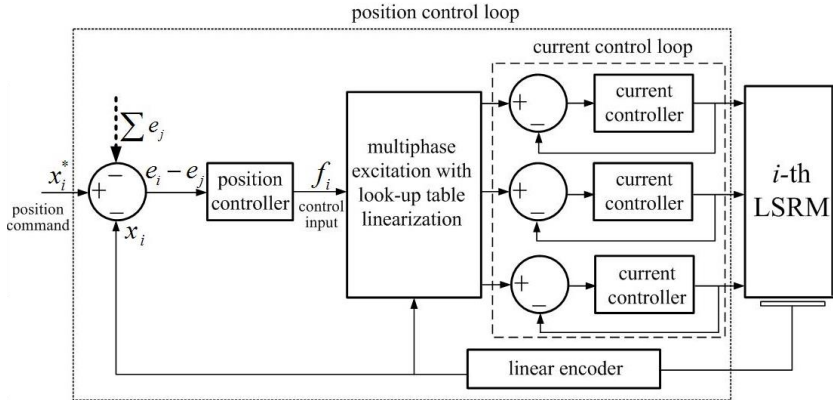

Figure 4. Unit system control scheme.

3.3. Coordinated Tracking Control Module

The extended second-order continuous-time consensus algorithm is employed as the coordinated tracking control strategy [5] for the multiple LSRMs. The consensus algorithm for double-integrator dynamics is formulated as [9],

$$\ddot{x}_i = \ddot{x}_i^* - \alpha(e_i + \beta\dot{e}_i) - \sum_{j=1}^{N} a_{ij}\left[(e_i - e_j) + \beta(\dot{e}_i - \dot{e}_j)\right] \tag{4}$$

where $e_i = x_i - x_i^*$ and $e_j = x_j - x_j^*$ denote the difference between the actual and the desired position from the i-th and the j-th unit system, respectively. α and β are positive scalar gains and a_{ij} is the (i, j) entry of the adjacency matrix $A \in R^{N\times N}$ associated with graph G modeling the communication topology among multiple LSRMs. To save communication resources, the same communication links can be shared for both the upper and the lower level. In this paper, the communication topology of reference signal agreement associated with $\hat{A}$ can be represented as A. The dynamics of the LSRM based motion control system in (1) can also be expressed as,

$$\ddot{x}_i = -\frac{B_i}{m_i}\dot{x}_i - \frac{1}{m_i}fl_i + \frac{1}{m_i}f_i \tag{5}$$

Substituting (4) into (5), the control input for the i-th LSRM system can be obtained as,

$$f_i = \underbrace{B_i \frac{dx_i}{dt} + fl_i}_{\text{model compensation}} \underbrace{+ m_i \ddot{x}_i^* - m_i \alpha (e_i + \beta \dot{e}_i) - m_i \sum_{j=1}^{N} a_{ij} \left[(e_i - e_j) + \beta (\dot{e}_i - \dot{e}_j) \right]}_{\text{tracking synchronization}} \tag{6}$$

It is clear that the control input comprises the model compensation term and the tracking synchronization term. The former is used to compensate the dynamics in the i-th unit system, and the latter urges the i-th LSRM to track the i-th reference signal and coordinate with other LSRMs.

3.4. Stability Analysis

After substituting (6) into (5), we can obtain the closed-loop dynamics of the tracking error for the i-th LSRM as,

$$\ddot{e}_i = -\alpha e_i - \sum_{j=1}^{N} a_{ij} (e_i - e_j) - \beta \alpha \dot{e}_i - \beta \sum_{j=1}^{N} a_{ij} (\dot{e}_i - \dot{e}_j) \tag{7}$$

The closed loop dynamics of the tracking error for the network can be reformulated in the matrix form as,

$$\begin{bmatrix} \dot{e} \\ \ddot{e} \end{bmatrix} = \begin{bmatrix} 0_N & I_N \\ -(\alpha I_N + L) & -\beta(\alpha I_N + L) \end{bmatrix} \begin{bmatrix} e \\ \dot{e} \end{bmatrix} \tag{8}$$

where $e = [e_1 \quad e_2 \quad \dots \quad e_N]^T$ is the error vector from all the machines and 0_N and I_N denote the N by N full zero matrix and the identity matrix, respectively. $L \in R^{N \times N}$ is the Laplacian matrix with respect to G. Let,

$$\Lambda = \begin{bmatrix} 0_N & I_N \\ -(\alpha I_N + L) & -\beta(\alpha I_N + L) \end{bmatrix} \tag{9}$$

According to linear system theory, the necessary and sufficient condition ensuring the stability of the close-loop system (8) is that all of the eigenvalues of matrix Λ must have negative real parts, as follows,

$$\mathrm{Re}[\lambda_i(\Lambda)] < 0, i = 1, \dots, N \tag{10}$$

where λ_i is the i-th eigenvalue of matrix Λ. $\mathrm{Re}(\cdot)$ and $\mathrm{Im}(\cdot)$ denote the real and imaginary parts of a complex number, respectively.

Lemma 1. *Given the matrix* $M = \begin{bmatrix} A & B \\ C & D \end{bmatrix}$, *if block matrix A and C commute, it satisfies that* $\det(M) = \det(AD - CB)$, *where* $\det(\cdot)$ *represents the determinant of a matrix [20].*

According to *Lemma* 1, the characteristic polynomial of Λ is given by,

$$\begin{aligned} \det(\lambda I_{2N} - \Lambda) &= \det\left(\begin{bmatrix} \lambda I_N & -I_N \\ (\alpha I_N + L) & \lambda I_N + \beta(\alpha I_N + L) \end{bmatrix} \right) \\ &= \det\left[\lambda^2 I_N + (1 + \beta\lambda)(\alpha I_N + L) \right] \end{aligned} \tag{11}$$

According to the definition of a matrix eigenvalue, (11) can further be reformulated as,

$$\det\left[\lambda^2 I_N + (1 + \beta\lambda)(\alpha I_N + L) \right] = \prod_{i=1}^{N} \left(\lambda_i^2 - (1 + \beta\lambda_i)\kappa_i \right) \tag{12}$$

where $\kappa_i = -\alpha + \mu_i, i = 1, \ldots, N$ is the eigenvalues of $-(\alpha I_N + L)$ and $\mu_i, i = 1, \ldots, N$ represents the i-th eigenvalues of $-L$. Equation (12) indicates that the roots of the characteristic polynomial of Λ can be obtained by solving $\lambda_i^2 - (1 + \beta\lambda_i)\kappa_i = 0$. Therefore, the eigenvalues of Λ can be given by,

$$\begin{aligned} \lambda_{i\pm} &= \frac{\beta(\mu_i - \alpha) \pm \sqrt{\beta^2(\mu_i - \alpha)^2 + 4(\mu_i - \alpha)}}{2} \\ &= \frac{\beta\kappa_i \pm \sqrt{\beta^2\kappa_i^2 + 4\kappa_i}}{2} \end{aligned} \tag{13}$$

where λ_{i-} and λ_{i+} are the eigenvalues of Λ associated with κ_i, μ_i.

For any directed graph G, all nonzero eigenvalues of the Laplacian matrix L associated with the graph G have positive real parts, that is, the eigenvalues μ_i of $-L$ satisfy $\mathrm{Re}(\mu_i) \leq 0$. Especially, the matrix $-L$ has a simple zero eigenvalue and all other eigenvalues have negative real parts when the graph G has a directed spanning tree [4]. Hence, we can see $\mathrm{Re}(\kappa_i) = \mathrm{Re}(-\alpha + \mu_i) < 0, i = 1, \ldots, N$ for any directed graph. Therefore, the real parts $\mathrm{Re}(\lambda_{i\pm})$ of the eigenvalues $\lambda_{i\pm}$ of matrix Λ can be investigated according to the eigenvalues κ_i of $-(\alpha I_N + L)$. If $\mathrm{Re}(\kappa_i) < 0$ and $\mathrm{Im}(\kappa_i) = 0$, namely $\kappa_i < 0$, then the eigenvalues of Λ satisfy obviously $\mathrm{Re}[\lambda_i(\Lambda)] < 0, i = 1, \ldots, N$ for any $\beta > 0$, where $\lambda_{i\pm}$ are the eigenvalues of Λ associated with κ_i. Besides, if $\mathrm{Re}(\kappa_i) < 0$ and $\mathrm{Im}(\kappa_i) \neq 0$, it needs to be considered only that κ_i satisfies $\mathrm{Re}(\kappa_i) < 0$ and $\mathrm{Im}(\kappa_i) > 0$, because any κ_i that satisfies $\mathrm{Re}(\kappa_i) < 0$ and $\mathrm{Im}(\kappa_i) < 0$ is a complex conjugate of κ_i that satisfies $\mathrm{Re}(\kappa_i) < 0$ and $\mathrm{Im}(\kappa_i) > 0$ [20]. In order to guarantee that all eigenvalues of Λ possess negative real parts, the following lemma is applied for obtaining the condition that β should satisfy under $\mathrm{Re}(\kappa_i) < 0$ and $\mathrm{Im}(\kappa_i) > 0$.

Lemma 2. *Given*

$$\rho_\pm = \frac{\gamma\eta \pm \sqrt{\gamma^2\eta^2 + 4\eta}}{2} \tag{14}$$

where ρ and η denote two complex numbers and γ is a constant coefficient. If $\mathrm{Re}(\eta) < 0$, $\mathrm{Im}(\eta) > 0$ *and:*

$$\gamma > \sqrt{\frac{2}{|\eta| \cos\left(\frac{\pi}{2} - \tan^{-1}\frac{-\mathrm{Re}(\eta)}{\mathrm{Im}(\eta)}\right)}} \tag{15}$$

then $\mathrm{Re}(\rho_\pm) < 0$.

According to *Lemma* 2, the conclusion can be drawn directly that $\lim_{t\to\infty} \|e\| = 0$ and $\lim_{t\to\infty} \|\dot{e}\| = 0$ can be satisfied for any graph G, if the scale gain α, β meet the following conditions:
Case 1: Gain β satisfies $\beta > 0$, if κ_i associated with all the eigenvalues μ_i of $-L$ meets $\mathrm{Re}(\kappa_i) < 0$ and $\mathrm{Im}(\kappa_i) = 0$.
Case 2: β satisfies,

$$\beta > \max_{\substack{\forall \mathrm{Re}(\mu_i - \alpha) < 0 \\ \& \ \mathrm{Im}(\mu_i - \alpha) > 0}} \sqrt{\frac{2}{|\mu_i - \alpha| \cos\left(\frac{\pi}{2} - \tan^{-1}\frac{-\mathrm{Re}(\mu_i - \alpha)}{Im(\mu_i - \alpha)}\right)}} \tag{16}$$

if κ_i meets $\mathrm{Re}(\kappa_i) < 0$ and $\mathrm{Im}(\kappa_i) \neq 0$.

Remark 1. *From the above mentioned stability analysis, the tracking synchronization algorithm degrades to the independent tracking control of each LSRM in spite of the non-existence of any network topology. However, the tracking synchronization algorithm still ensures that each LSRM can correctly follow its reference signal individually. It can also be concluded that the proposed low-level tracking synchronization scheme guarantees both the tracking and coordination performance of LSRMs, if there is a spanning tree in the graph. Generally speaking, a network topology often guarantees more than one direct spanning tree if there exists redundant edges.*

Therefore, the loss of communication links will not affect the existence of direct spanning trees. From the above analysis, the control structure owns certain fault-tolerance ability.

4. Network Construction

4.1. Simulation Analysis

The control block diagram according to the above analysis can be represented as shown in Figure 5a. The entire control strategy is divided in two parts, the upper-level reference agreement and the lower-level coordination synchronization, respectively. The reference parameters such as amplitude, frequency, and phase values are unified in the signal agreement block based on the first-order consensus algorithm. In the lower-level, the coordinated controller f_i for each LSRM is derived from the second-order consensus algorithm. In addition, the coordinated controllers realize the reference signal tracking synchronization through the communication topology.

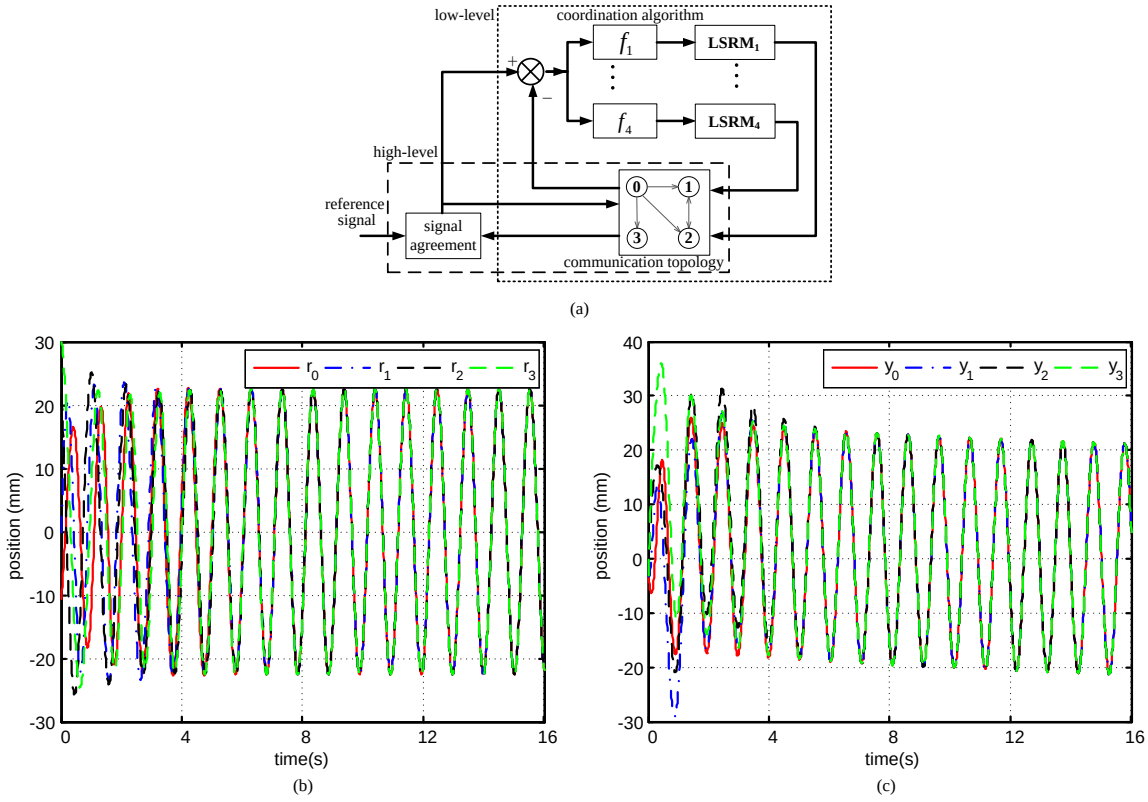

Figure 5. (**a**) control block diagram of the LSRMs network, (**b**) simulation results of reference, and (**c**) actual signals.

The *cycle* topology is applied for the agreement of the reference signals, as shown in Figure 5b. The *tree* communication network topology is utilized for the synchronization of the four machines according to Figure 5c. Table 2 tabulates the control parameters and eigenvalues associated with $-L$ and Λ, respectively, according to the constraints from Case 1. It can be verified by stability analysis above that all the parameters from Table 2 fall into the scope of stability. Table 3 defines the parameters.

Table 2. Controller Gains

Symbol	Value
α	1
β	1
μ	$[-1 \quad -1 \quad -1 \quad 0]$
λ	$[-1 \pm i \quad -1 \pm i \quad -1 \pm i \quad -0.5 \pm 0.866i]$

Table 3. Parameter Definitions

LSRM	Reference Signal	Actual Signal	Error	Relative Reference	Relative Position
$i, j = 0, 1, 2, 3$			$r_i - y_i$	$r_i - r_j$	$y_i - y_j$
0	r_0	y_0	$error_0$	$errf_{01}$	$erry_{01}$
1	r_1	y_1	$error_1$	$errf_{02}$	$erry_{02}$
2	r_2	y_2	$error_2$	$errf_{03}$	$erry_{03}$
3	r_3	y_3	$error_3$	$errf_{12}$	$erry_{12}$
				$errf_{13}$	$erry_{13}$
				$errf_{23}$	$erry_{23}$

The reference signals for the four LSRMs are sinusoidal waveforms with parameters arbitrarily selected: the amplitudes are 15, 20, 25, and 30 mm and the frequency values are 5, 6, 6.5, and 7 rad/s with initial phase values of $-45°$, $0°$, $60°$, and $90°$, respectively. It is clear that the position command signals are strongly asynchronous from each other. As shown in Figure 5b,c the simulation results, it is clear that the regulation time for reference signal agreement and actual output response are about 4.2 s and 4.5 s, respectively.

4.2. Experimental Setup

The networked control platforms utilize two dSPACE DS1104 boards with on-board 250 MHz floating-point processors. The control boards directly interface with the Real-Time Workshop of MATLAB/SIMULINK (R2015a, MathWorks, Natick, Massachusetts, USA) and all control parameters can be modified online. Each control board connects two LSRMs and it has two 24-bit incremental encoder channels, six channels of 12-bit digital-to-analog interface, two serial ports, and several input/output connection pins. The control platforms communicate with each other through the serial port interface.

Each closed loop unit position control system is composed of the LSRM, dSPACE interface, amplifiers, linear magnetic encoder, and power supply with transformers. As shown in Figure 6a the experimental setups, each LSRM employs three commercial amplifiers for current loop regulation with a 10 kHz switching frequency based on the proportional integral algorithm. As shown in Figure 6b, the stators of the four LSRMs are fixed on an aluminum shelf and the linear magnetic encoders with the resolution of 1 μm are mounted on the encoder brackets.

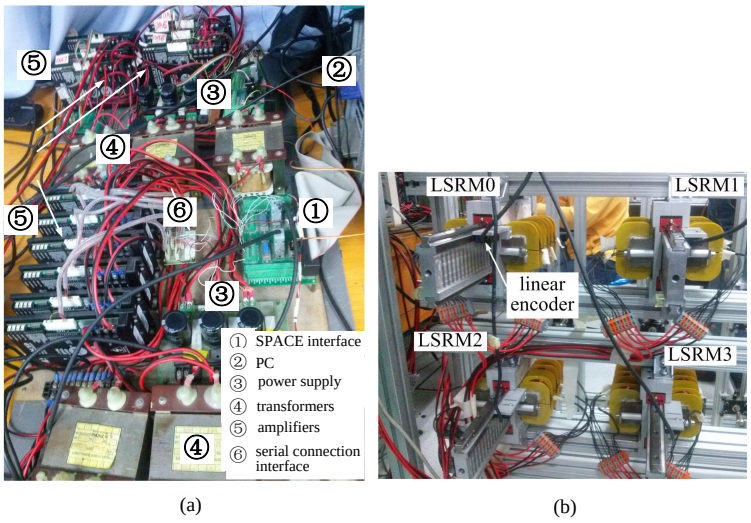

Figure 6. experimental setup: (**a**) power supplies, drivers, controllers and (**b**) the LSRMs.

4.3. Network Configuration

The *tree* communication network topology from Figure 2b is realized as hardware as depicted in Figure 7. Since each dSPACE control platform manages two LSRMs, communication between unit system 0 to 1 is realized by direct connection without considering any communication data delays or dropouts. However, the communication between unit system 0 to 2 and 3 are realized by the serial port with RS232 protocol. The baud rate is 57,600 with data and stop bit set as 8 and 1, respectively.

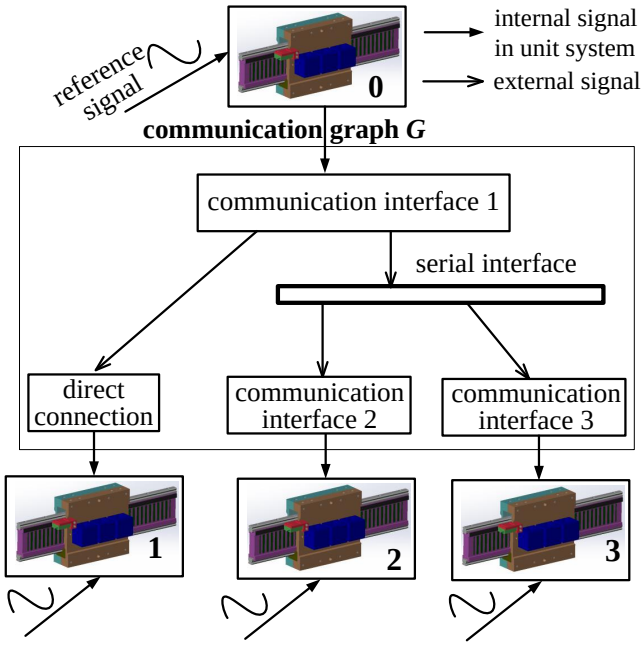

Figure 7. Hardware communication.

5. Experimental Results

For clear illustration of the independent and coordinated tracking behaviors of each machine, Table 3 defines the indices that characterize the control performance. Independent tracking behaviors of any machine can be represented by; $error_i$, since it represents the error response from the reference

signal r_i to its actual output y_i of the i-th machine; relative reference $err\,f_{ij}$ illustrates the synchronization performance between the i-th and j-th reference signal; and relative position $erry_{ij}$ depicts the coordination behavior between the i-th and j-th LSRM.

5.1. Control Performance under Two-level Tracking Control

The dynamic position response waveforms under the proposed hierarchical synchronization scheme can be found in Figure 8. From Figure 8a, it is clear that the reference signals from each LSRM successfully synchronize after 4.8 s. The dynamic profiles of the signal agreement correspond to those from simulation. Since there exist protection mechanisms to avoid collision from the stroke limit, the offset of the motion profiles is approximately zero. The actual output waveforms y for the four machines also synchronize since the four reference signals achieve agreement and the maximum error values fall below ± 2 mm from Figure 8b.

The relative reference profiles in Figure 8c further demonstrate the agreement of the four reference signals. The relative position waveforms between any two LSRMs are illustrated in Figure 8d. It can be concluded that the four machines have achieved coordinated tracking after the agreement of the reference signals. The results prove the successful tracking coordination of four LSRMs under asynchronous reference signals by employing the proposed hierarchical, two-level synchronization strategy.

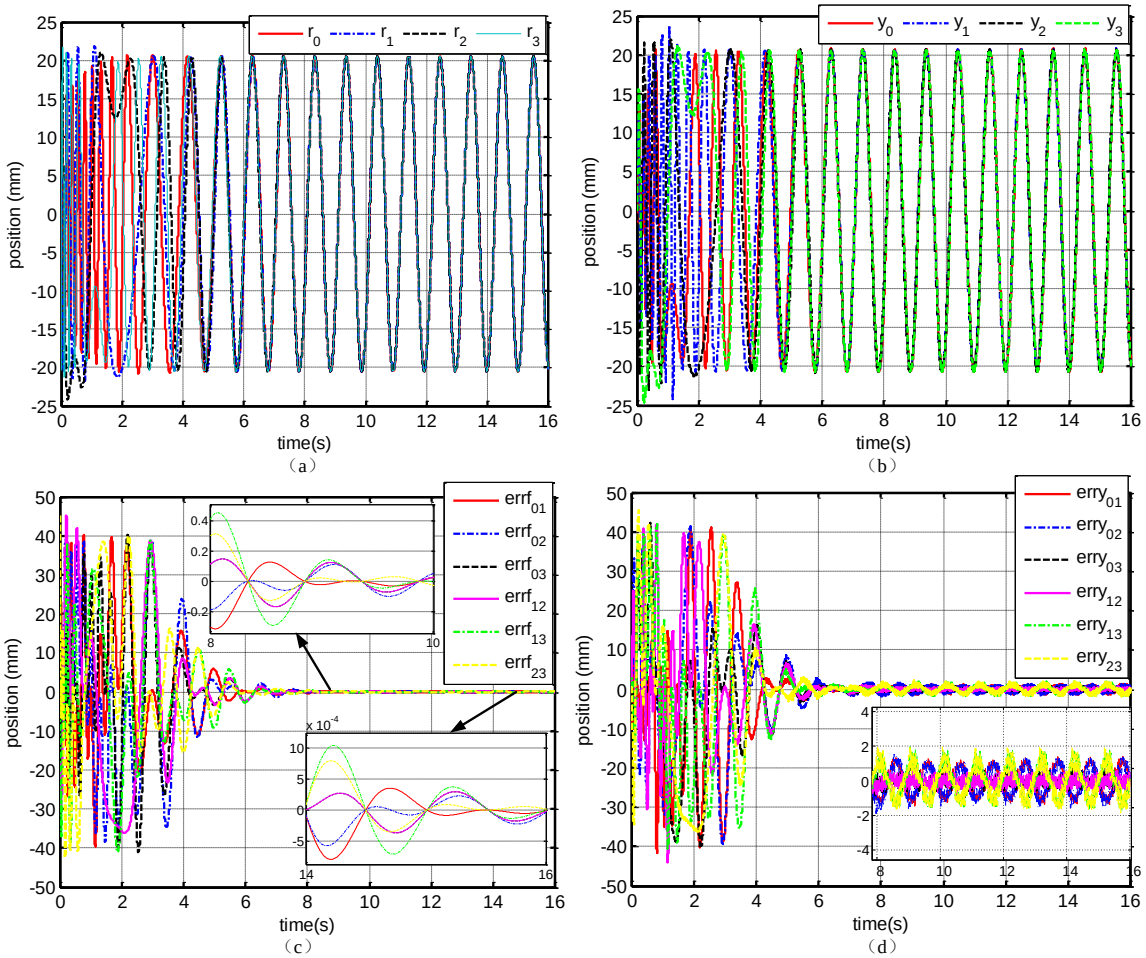

Figure 8. Dynamic position response waveforms: (**a**) reference, (**b**) actual and (**c**) relative reference, and (**d**) relative position signals under hierarchical synchronization.

5.2. Performance under Lower-Level Tracking

It can be seen from Figure 9a,b that each LSRM is capable of independent tracking according to its position reference signal. In addition, $error_2$ and $error_3$ are higher from LSRM2 and LSRM3 than $error_0$ and $error_1$ from LSRM0 and LSRM1, since communication dropouts or delays, etc., inevitably affect the performance of LSRM2 and LSRM3. The experimental results from Figure 9c also demonstrate that as the reference agreement disappears, the lower-level, coordination synchronization algorithm is not capable of proper tracking coordination of the LSRMs, due to the fact that each LSRM follows its own reference signal, which serves as a strong external disturbance to other LSRMs. Therefore, without reference signals agreement, the lower-level tracking control only ensures independent tracking instead of coordinated tracking performance.

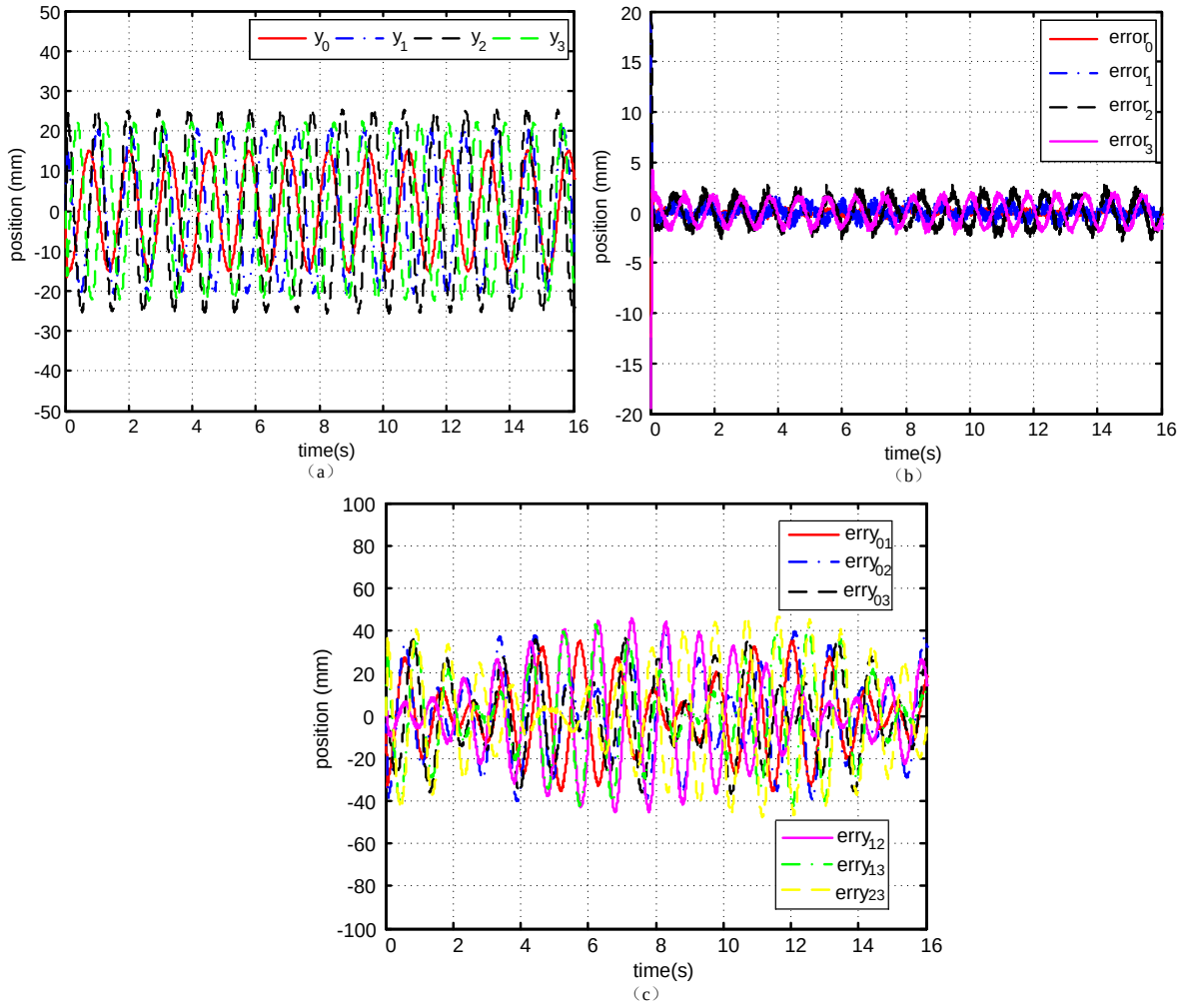

Figure 9. Dynamic position response waveforms: (**a**) actual, (**b**) error, and (**c**) relative position signals under low-level tracking synchronization.

5.3. Performance under Independent Tracking

Figure 10 presents the output performance under four different reference signals when both upper-level reference agreement and lower-level, coordinated tracking control disappear. This simulates the situation that all synchronization strategies fail. The control strategy now degrades to independent tracking of the reference signal of their own with no coordination among the four machines. It can be seen that each LSRM strictly follows its own reference signal only, and the response

profiles are similar to the dynamic waveforms of relative position under the lower-level control strategy only.

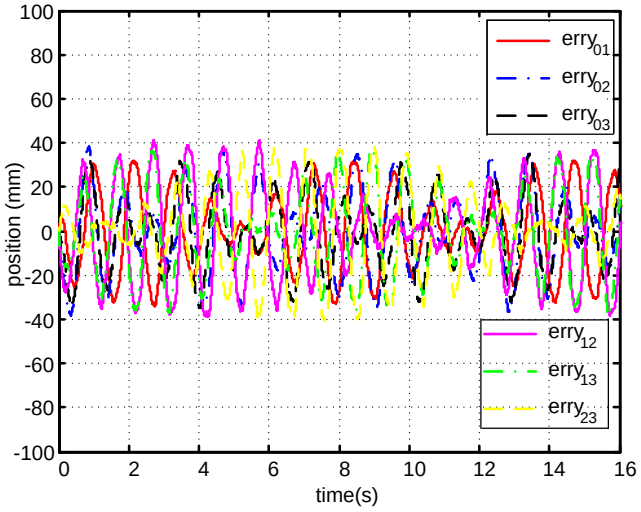

Figure 10. Dynamic position response waveforms of relative signals under independent tracking control scheme.

6. Conclusions and Discussion

Based on the actual requirements of coordination of reference signals for linear machines, this paper investigates a hierarchical, two-level synchronization control strategy for four coordinated tracking control of direct-drive, double-sided asymmetric LSRMs. The proposed fault-tolerant, hierarchical coordination control strategy ensures the coordinated tracking performance of LSRMs if there exists a spanning tree in the network topology modeled by the graph. In addition, independent tracking performance can be ensured in spite of any communication among LSRMs. Comparative study demonstrates that successful coordinated tracking control takes the premise of the agreement of reference signals, since asynchronous command signals serve as strong external disturbances to other unit systems.

The applications of the four synchronized direct-drive, LSRMs can be targeted for the implementation of the multi-processing line. The proposed hierarchical synchronization control strategy ensures the smooth operation of the processing line with certain position control precision. It can be expected that the proposed synchronization strategy is also suitable for the cooperative operation of multiple rotary or linear electric machines that require position or force coordination among machines.

Future research will focus on the implementation of the proposed algorithm on four digital, single-chip processors such as digital signal processors to further reduce performance deterioration due to communication limitations among unit systems. From current study, there lacks any closed control scheme for the entire group system globally, since the information from each LSRM does not provide any feedback to the network. Therefore, global closed loop control strategies are suggested to be considered for further improvement of the synchronization motion control performance.

Acknowledgments: This work was supported in part by the National Natural Science Foundation of China under Grant 51477103, 51577121, 11572248, 61690211 and 61403258.The authors also would like to thank Guangdong and Shenzhen Government under the code of S2014A030313564, 2015A010106017, 2016KZDXM007, JCYJ20160308104825040 and JCYJ20170302145012329 for support.

Author Contributions: Bo Zhang and J.F. Pan conceived and wrote the paper main body and designed the main body of study. Jianping Yuan and Xiaoyu Wu guide the system designed, analyzed the data and revised the manuscript. Li Qiu performed the simulations and experiments. Jianjun Luo helped to revise the paper.

Conflicts of Interest: The authors declare no conflict of interest.

References

1. Olfati-Saber, R.; Fax, J.A.; Murray, R.M. Consensus and cooperation in networked multi-agent systems. *Proc. IEEE* **2007**, *95*, 215–233.
2. Zhang, H.; Lewis, F.L.; Qu, Z. Lyapunov, adaptive, and optimal design techniques for cooperative systems on directed communication graphs. *IEEE Trans. Ind. Electron.* **2012**, *59*, 3026–3041.
3. Movric, K.H.; Lewis, F.L. Cooperative optimal control for multi-agent systems on directed graph topologies. *IEEE Trans. Autom. Control* **2014**, *59*, 769–774.
4. Cao, Y.; Ren, W. Multi-vehicle coordination for double-integrator dynamics under fixed undirected/directed interaction in a sampled-data setting. *Int. J. Robust Nonlinear Control* **2010**, *20*, 981–1000.
5. Ren, W. On consensus algorithms for double-integrator dynamics. *IEEE Trans. Autom. Control* **2008**, *58*, 1503–1509.
6. Cao, Y.; Yu, W.; Ren, W.; Chen, G. An overview of recent progress in the study of distributed multi-agent coordination. *IEEE Trans. Ind. Inform.* **2013**, *9*, 427–438.
7. Egerstedt, M.; Martini, S.; Cao, M.; Camlibel, K.; Bicchi, A. Interacting with networks: how does structure relate to controllability in single-leader consensus networks? *Control Syst. Mag.* **2012**, *32*, 2137–2146.
8. Yu, W.; Zhou, L.; Yu, X.; Lu, J.; Lu, R. Consensus in multi-agent systems with second-order dynamics and sampled data. *IEEE Trans. Ind. Inform.* **2013**, *9*, 66–73.
9. Li, Z.; Wen, G.; Duan, Z.; Ren, W. Designing fully distributed consensus protocols for linear multi-agent systems with directed graphs. *IEEE Trans. Autom. Control* **2015**, *60*, 1152–1157.
10. Qu, Z.; Wang, J.; Hull, R.A. Cooperative control of dynamical systems with application to autonomous vehicles. *IEEE Trans. Autom. Control* **2008**, *53*, 894–911.
11. Li, Z.; Liu, H.; Zhu, B.; Gao, H. Robust second-order consensus tracking of multiple 3-DOF laboratory helicopters via output feedback. *IEEE/ASME Trans. Mechatron.* **2015**, *20*, 2538–2549.
12. Szabo, L.; Viorel, I.A.; Chisu, I.; Kovacs, Z. A novel double salient permanent magnet linear motor. In Proceedings of the International Conference on Power Electronics, Drives and Motion (PCIM), Nürnberg, Germany, 1999.
13. Zhang, B.; Yuan, J.; Qiu, L.; Cheung, N.; Pan, J.F. Distributed coordinated motion tracking of the linear switched reluctance machines based group control system. *IEEE Trans. Ind. Electron.* **2016**, *63*, 1480–1489.
14. Pan, J.F.; Zou, Y.; Cao, G. An asymmetric linear switched reluctance motor. *IEEE Trans. Energy Convers.* **2013**, *28*, 444–451.
15. Park, J.; Jang, S.; Choi, J.; Sung, S.; Kim, I. Dynamic and experimental performance of linear-switched reluctance machine with inductance variation according to airgap length. *IEEE Trans. Mag.* **2010**, *46*, 2334–2337.
16. Amoros, J.G.; Andrada, P. Sensitivity analysis of geometrical parameters on a double-sided linear switched reluctance motor. *IEEE Trans. Ind. Electron.* **2010**, *57*, 311–319.
17. Lin, J.; Cheng, K.W.E.; Zhang, Z.; Cheung, N.C.; Xue, X.; Ng, T. Active suspension system based on linear switched reluctance actuator and control schemes. *IEEE Trans. Veh. Technol.* **2013**, *62*, 562–572.
18. Pan, J.F.; Zou, Y.; Cao, G. Adaptive controller for the double-sided linear switched reluctance motor based on the nonlinear inductance modelling. *IET Electr. Power Appl.* **2013**, *7*, 1–15.
19. Mesbahi, M.; Egerstedt, M. *Graph Theoretic Methods for Multiagent Networks*; Princeton University Press: Princeton, NJ, USA, 2010; Chapter 6.
20. Ren, W.; Beard, R.W. *Distributed Consensus in Multi-Vehicle Cooperative Control*; Springer: London, UK, 2008; Chapters 3–4.
21. Ren, W.; Atkins, E. Distributed multi-vehicle coordinated control via local information exchange. *Int. J. Robust Nonlinear Control* **2007**, *17*, 1002–1033 .